Biomedical Optics EXPRESS

Optical tractography of the mouse heart using polarization-sensitive optical coherence tomography

Yuanbo Wang and Gang Yao*

Department of Bioengineering, University of Missouri, Columbia, MO, 65201, USA
yaog@missouri.edu

Abstract: We developed a method to image myocardial fiber architecture in the mouse heart using a Jones matrix-based polarization-sensitive optical coherence tomography (PSOCT) system. The "cross-helical" laminar structure of myocardial fibers can be clearly visualized using this technology. The obtained myocardial fiber organization agrees well with existing knowledge acquired using conventional histology and diffusion tensor magnetic resonance imaging.

OCIS codes: (110.4500) Optical coherence tomography; (230.5440) Polarization.

References and links

1. D. D. Streeter, Jr., H. M. Spotnitz, D. P. Patel, J. Ross, Jr., and E. H. Sonnenblick, "Fiber orientation in the canine left ventricle during diastole and systole," Circ. Res. **24**(3), 339–347 (1969).
2. D. D. Streeter and D. L. Bassett, "An engineering analysis of myocardial fiber orientation in pig's left ventricle in systole," Anat. Rec. **155**(4), 503–511 (1966).
3. I. J. LeGrice, B. H. Smaill, L. Z. Chai, S. G. Edgar, J. B. Gavin, P. J. Hunter, "Laminar structure of the heart: ventricular myocyte arrangement and connective tissue architecture in the dog," Am. J. Physiol.-Heart. C. **269**(2 38–2), H571–582 (1995).
4. B. Taccardi, E. Macchi, R. L. Lux, P. R. Ershler, S. Spaggiari, S. Baruffi, and Y. Vyhmeister, "Effect of myocardial fiber direction on epicardial potentials," Circulation **90**(6), 3076–3090 (1994).
5. I. J. LeGrice, Y. Takayama, and J. W. Covell, "Transverse shear along myocardial cleavage planes provides a mechanism for normal systolic wall thickening," Circ. Res. **77**(1), 182–193 (1995).
6. G. J. Strijkers, A. Bouts, W. M. Blankesteijn, T. H. J. M. Peeters, A. Vilanova, M. C. van Prooijen, H. M. H. F. Sanders, E. Heijman, and K. Nicolay, "Diffusion tensor imaging of left ventricular remodeling in response to myocardial infarction in the mouse," NMR Biomed. **22**(2), 182–190 (2009).
7. D. E. Sosnovik, R. Wang, G. Dai, T. G. Reese, and V. J. Wedeen, "Diffusion MR tractography of the heart," J. Cardiovasc. Magn. Reson. **11**(1), 47–61 (2009).
8. C. P. Fleming, C. M. Ripplinger, B. Webb, I. R. Efimov, and A. M. Rollins, "Quantification of cardiac fiber orientation using optical coherence tomography," J. Biomed. Opt. **13**(3), 030505 (2008).
9. C. M. Ambrosi, V. V. Fedorov, R. B. Schuessler, A. M. Rollins, and I. R. Efimov, "Quantification of fiber orientation in the canine atrial pacemaker complex using optical coherence tomography," J. Biomed. Opt. **17**(7), 071309 (2012).
10. C. J. Goergen, H. Radhakrishnan, S. Sakadžić, E. T. Mandeville, E. H. Lo, D. E. Sosnovik, and V. J. Srinivasan, "Optical coherence tractography using intrinsic contrast," Opt. Lett. **37**(18), 3882–3884 (2012).
11. C. Fan and G. Yao, "Mapping local retardance in birefringent samples using polarization sensitive optical coherence tomography," Opt. Lett. **37**(9), 1415–1417 (2012).
12. C. Fan and G. Yao, "Mapping local optical axis in birefringent samples using polarization-sensitive optical coherence tomography," J. Biomed. Opt. **17**(11), 110501 (2012).
13. C. Fan and G. Yao, "Imaging myocardial fiber orientation using polarization sensitive optical coherence tomography," Biomed. Opt. Express **4**(3), 460–465 (2013).
14. C. Fan and G. Yao, "Full-range spectral domain Jones matrix optical coherence tomography using a single spectral camera," Opt. Express **20**(20), 22360–22371 (2012).
15. Y. Jiang, K. Pandya, O. Smithies, and E. W. Hsu, "Three-dimensional diffusion tensor microscopy of fixed mouse hearts," Magn. Reson. Med. **52**(3), 453–460 (2004).
16. L. J. Healy, Y. Jiang, and E. W. Hsu, "Quantitative comparison of myocardial fiber structure between mice, rabbit, and sheep using diffusion tensor cardiovascular magnetic resonance," J. Cardiovasc. Magn. Reson. **13**(1), 74 (2011).
17. C. Mekkaoui, S. Huang, H. H. Chen, G. Dai, T. G. Reese, W. J. Kostis, A. Thiagalingam, P. Maurovich-Horvat, J. N. Ruskin, U. Hoffmann, M. P. Jackowski, and D. E. Sosnovik, "Fiber architecture in remodeled myocardium

#195629 - $15.00 USD Received 12 Aug 2013; revised 13 Oct 2013; accepted 15 Oct 2013; published 21 Oct 2013

revealed with a quantitative diffusion CMR tractography framework and histological validation," J. Cardiovasc. Magn. Reson. **14**(1), 70 (2012).
18. R. H. Clayton, S. Abdalhamid, R. Bloor, G. Kyprianou, K. Kotagiri, J. Lee, A. Mane, and R. White, "Transmural changes in fibre helix angle in normal and failing canine ventricles," Comput. Cardiol. **37**, art. 5738123, 915–918 (2010).
19. W. J. Karlon, J. W. Covell, A. D. McCulloch, J. J. Hunter, and J. H. Omens, "Automated measurement of myofiber disarray in transgenic mice with ventricular expression of ras," Anat. Rec. **252**(4), 612–625 (1998).

1. Introduction

Histological studies [1, 2] have revealed the "cross-helical" structure of myocardial fibers formed laminarly at different transmural thicknesses in the ventricular myocardium of the heart [3]. This unique fiber architecture has a great influence on mechanical and electrical heart functions [4, 5]. Abnormal fiber organization is linked to cardiac dysfunction and alterations in cardiac muscle structure have been found as a result of myocardial infarction [6]. Therefore "tractography", an imaging tool that can acquire microstructural details of tissue fiber organization, is valuable for both basic research and clinical diagnosis. Despite its superior spatial resolution, histological assessment is time consuming and limited to imaging of small areas. Alternatively, diffusion-tensor magnetic resonance imaging (DTI) [7] has been established as a state-of-art method for imaging the 3D fiber organization in whole hearts; however, the image resolution in DTI is usually limited to submillimeters.

Optical coherence tomography (OCT) is a non-destructive optical imaging technique that can provide depth-resolved high resolution tissue images at high speed. It has been shown that ultrahigh resolution OCT can be used to acquire fiber orientation in heart tissue using intensity contrast [8–10]. Because fibrous tissues such as myocardium show intrinsic optical birefringence, fiber orientation can be estimated using the optical axis' information. Recently, a set of algorithms [11–13] have been developed to extract the depth-resolved local optical polarization properties from polarization-sensitive optical coherence tomography (PSOCT) images. Fan and Yao [13] demonstrated that these algorithms can be applied in a Jones matrix PSOCT system [14] to visualize myocardial fiber orientation in a piece of bovine heart tissue.

Here, we further extend our previous studies by developing a new scanning and image reconstruction procedure to acquire tractography in whole mouse hearts. The well-known "cross-helical" laminar structure of myocardial fibers in the ventricular myocardium can be clearly visualized using this technology and the obtained myocardial fiber organization agreed well with existing knowledge acquired using diffusion tensor magnetic resonance imaging.

2. Method

The Jones matrix PSOCT system used in this study is a single camera-based full-range spectral domain system as described in detail in [13]. This system was carefully calibrated for imaging conventional 'cumulative' polarization properties including retardance (or 'phase retardation'), optical axis and diattenuation [13]. A Superluminescent Light Emitting Diode (SLD) was used as the light source (SLD-351-HP, Superlum, Ireland) at a central wavelength of 847.8 nm. The system had a depth resolution of 8.2 μm in the air within 1.5 mm of the zero delay line as characterized using the interference signal from a mirror at the sample arm. The lateral resolution of the system was 12.4 μm when measured using a 1951 USAF test target. All size/distance values presented in this report were measured in air.

The excised mouse heart was fixed in 4% paraformaldehyde and imaged *ex vivo*. A 20 gauge needle was used to hold the heart by passing through the heart apex and center of the base. The needle was mounted on a rotational stage (PRM1Z8, Thorlabs, Inc., Newton, New Jersey, USA) and was aligned with the rotational axis. The stage was rotated continuously over 270° at a speed of 1.25°/sec. This rotation range was chosen to ensure that the entire left ventricle and part of the right ventricle can be imaged within the effective image depth of 2.6 mm of the PSOCT system [14]. A total of 2700 B-scans (2000 pixels in each B-scan covering

#195629 - $15.00 USD Received 12 Aug 2013; revised 13 Oct 2013; accepted 15 Oct 2013; published 21 Oct 2013

7.0 mm) were acquired at a speed of 12.5 B-scans per second (18μs camera exposure) to match the rotation speed. The entire scanning took 216 seconds to complete.

A coordinate system was set up to illustrate the measurement geometry as shown in Fig. 1. The incident light was aligned with the Z-axis (A-scan) and the B-scan was aligned with the Y-axis (parallel to the axis of rotation). The XY plane, i.e. the imaging plane for axis measurement, was perpendicular to the Z-axis and was set up as an analog to a histology slice. The projection angle of myocardial fibers passing through a pixel within the XY plane was measured by extracting the local (slow) optical axis in relation to the x-axis from the PSOCT images. The measured orientation θ had a range of [-90°, 90°] with positive angles inclined toward the positive x-axis (Fig. 1).

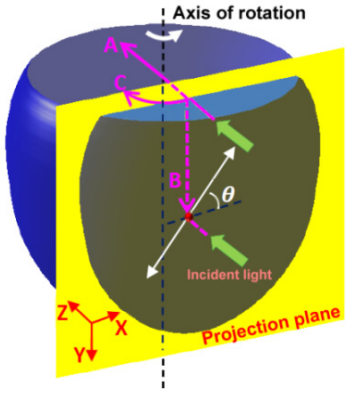

Fig. 1. An illustration of the imaging geometry. The incident light (A-scan) was aligned with the z-axis; the B-scan was along the axis of rotation (y-axis); and the heart sample was rotated for C-scan.

The procedure for extracting local optical axis, retardance and diattenuation from PSOCT was detailed in [13]. The term "optical axis" used here refers to the "slow" optical axis which is aligned with the fiber orientation. Briefly, the two orthogonal (horizontally and vertically polarized) components of the backscattered OCT signal were measured for both right- and left-handed circularly polarized incident light. The measured signals were stored in a "planar" 3D matrix of 650 × 2000 × 2700 pixels with pixel sizes of 5.4μm × 4μm × 7.9μm in A-, B-, and C-scans, respectively. A birefringent Jones matrix was constructed at each image pixel in the data set with tissue diattenuation removed by using only the real component of the measured complex retardance [13]. To improve signal-to-noise, the amplitudes of the two orthogonal polarization components and their phase difference were averaged over 3 consecutive B-scans during the calculation. In addition, a size three median filter (3 × 3 × 3) was applied to the 3D data set to further reduce speckle noise. Then, an iterative algorithm [12, 13] was used to calculate the local depth-resolved optical axis.

Figure 2 illustrates the procedure for constructing the 3D fiber tract from the local optical axis data set. The sample surface boundary was first obtained from the intensity data for each A-scan using a threshold-based segmentation algorithm [14]. Then, depth-resolved *en face* images were constructed from all pixels at a given transmural depth from the surface boundary (Fig. 2(a)). Examples of the extracted "planar" *en face* PSOCT images (intensity, local retardance, and optical axis) are shown in Fig. 2(b)-2(d). As shown in Fig. 2(c), the artery tissues (enclosed by the dashed line) had low retardance values which led to unreliable optical axis calculation. To focus on quantifying myocardial fibers in ventricles, the artery and atrium tissues were removed from further processing using a retardance threshold of 0.012 rad at the boundary of the ventricle as shown in Fig. 2(c)-2(e).

Within each *en face* image of the local optical axis (Fig. 2(d)), the stream2 function in Matlab was used to obtain the "streamline" representation of fiber tracts (Fig. 2(e)) [13]. A

#195629 - $15.00 USD Received 12 Aug 2013; revised 13 Oct 2013; accepted 15 Oct 2013; published 21 Oct 2013

uniform 25 × 34 mesh grid was used as the starting points in streamline calculation of the whole mouse heart. To improve the tractographic visualization, a cubic-spline interpolation algorithm was applied to each obtained fiber tract to fill the empty space between the tracking seeds so that each fiber tract contained 2700 points. The obtained fiber tract was further smoothed using an averaging filter with 1% of the given fiber length as the window size. To help eliminate incorrect fiber tracts produced by noisy data, short fiber tracts whose lengths were less than 5% of C-scan length were removed from visualization.

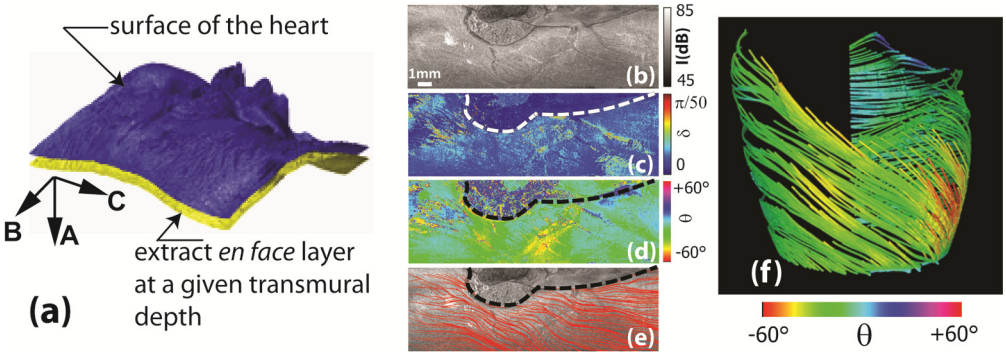

Fig. 2. An illustration of the procedure for reconstructing the tractography in a mouse heart. (a) Extracting an *en face* image at a given transmural depth. The planar presentation of the extracted *en face* images of (b) intensity, (c) local retardance, and (d) local fiber orientation; (e) the streamline presentation of fiber tract overlaying on the intensity image; (f) the reconstructed 3D tractographic representation of the fiber tracts in (e).

Once the "planar" orientation map (Fig. 2(e)) was obtained, it was then transformed into 3D coordinates using a polar transformation. The polar angle α_i at C-scan index i was computed as: $\alpha_i = (i / Nc) \times \Phi$, where N_C denotes the total number of C-scan and Φ is the full rotation range angle (270° in this study). The radius r in the polar transformation was computed as $r = R_0 - Surf(C_i, B_j, A_k)$, where R_0 denotes the maximum radius of the sample heart within the XZ plane (Fig. 1) and was 4.5 mm for the same presented here. $Surf(C_i, B_j, A_k)$ represents the depth of the image pixel at ith C-scan, jth B-scan, and kth A-scan in relation to R_0. An example of the obtained 3D tractographic representation is shown in Fig. 2(f). To better visualize the change in fiber orientation, fiber tracts were also displayed using a color map based on the orientation as shown in the color bar in Fig. 2(f).

All image processing was implemented using the Matlab software. The open source 3DSlicer (http://www.slicer.org/) was used for 3D data visualization.

3. Results and discussion

The 3D structure image of the whole mouse heart is shown in Fig. 3(a). Figure 3(c) to 3(e) show example B-scan images of the intensity, local retardance and axis extracted along the dashed line in Fig. 3(a). Clear optical axis information can be observed at a depth of 1.1 mm beneath the surface for most parts of the heart tissue, and up to 1.4 mm at some locations. As an assessment of the overall polarization properties, the average retardance and diattenuation were 2.8 ± 1.5 rad/mm and 1.2 ± 1.1 mm^{-1} in the left ventricle tissue over an area of 4.0 × 7.8 mm^2 (B × C) from 0.1 to 0.9 mm beneath the epicardium. The large variation suggested inhomogeneous polarization properties throughout the sample. We also noticed that the retardance value in mouse heart was smaller than that obtained in a piece of bovine heart [13].

The corresponding 3D tractograph is shown in Fig. 3(b). Please note that the atrium structure and arteries were removed from the fiber tracking as explained in the previous section. The laminar structure of the fiber orientation can be readily visualized from the color change: red color (negative orientation) at outside surface, and blue (zero degree) to pink

#195629 - $15.00 USD Received 12 Aug 2013; revised 13 Oct 2013; accepted 15 Oct 2013; published 21 Oct 2013

color (positive orientation) toward the inner surface. A more detailed examination of a small region of interest (ROI) extracted from the lateral side of the left ventricle is shown in Fig. 3(f)-3(i). The ROI had a size of 1.57 mm along the B-scan and covered 20° rotation along the C-scan (~1.6 mm in length). Sample images of the structure and local retardance/optical axis were shown at transmural depths from 0.11 mm to 0.91 mm. At small depths close to the heart surface the fibrous structures were vaguely recognizable at some locations in the intensity images and showed good agreement with the extracted local optical axis data. The rotation of the fiber orientation with transmural distance from epicardium to endocardium is revealed in Fig. 3(i). A "cross-helical" laminar structure is clearly formed by the negatively oriented fibers at 0.11 mm, circumferentially oriented (~0°) fibers at 0.51 mm, and positively oriented fibers at larger depths.

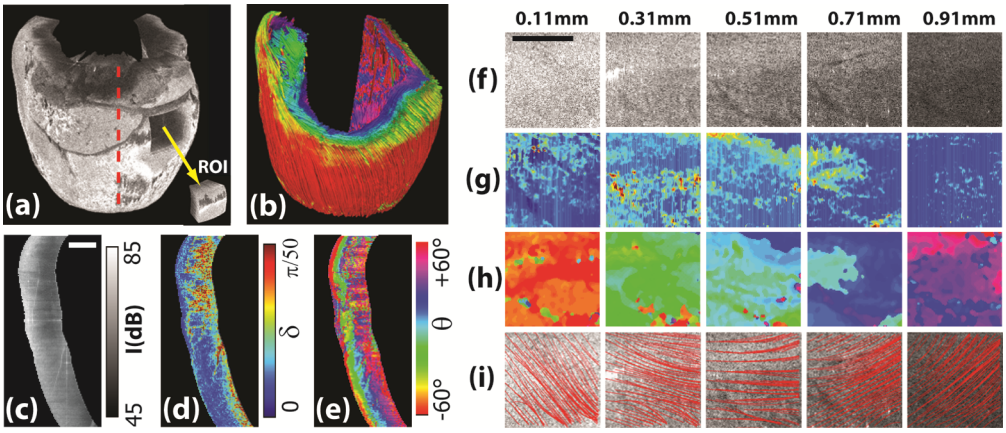

Fig. 3. (a) The 3D structure image of the mouse heart; (b) the corresponding 3D tractographic visualization. The B-scan images of structure, local retardance and optical axis acquired along the dashed line in (a) are shown in (c)-(e). Also shown are the *en face* images of the (f) structure, (g) local retardance, (h) local optical axis, and (i) cardiac fiber tract of a small region of interest (ROI) extracted at transmural depths from 0.11 mm to 0.91 mm. As shown in (a), the ROI was extracted from the lateral side of the left ventricle wall and had a size of 1.57 mm × 20° rotation (B × C-scan). The size bars in (c) and (f) are 1 mm.

Four additional small pieces of ROIs extracted at various left ventricle locations (Fig. 4) were quantified to examine the organization of myocardial fibers in the mouse heart. Each ROI had a size of 0.95 mm × 12° rotation (B-scan by C-scan). As shown in Fig. 4(a), the ROI-A, B, and C were located at the anterior, lateral, and posterior side of the left ventricle, respectively; whereas the ROI-D was located at the apical lateral wall of the left ventricle. Figure 4(b) shows the color-coded 3D tractography in the aforementioned four ROIs. A consistent transition in fiber orientation from negative angles (red color) at epicardium to positive angles (blue to pink color) toward endocardium can be seen.

The mean and standard deviation of the fiber orientation in the four aforementioned ROIs were computed and displayed as a function of the transmural depth in Fig. 4(c). The overall trend of these results was consistent with those reported in DTI studies [15, 16]. In all four ROIs, the fiber orientation exhibited the classic "cross-helical" structure, i.e. increasing monotonically from negative angles at epicardium to positive angles toward endocardium. The cardiac fibers were orientated at around −60° at depths close to epicardium, which is in good agreement with the values reported in both mice [15] and humans [17] using diffusion-tensor magnetic resonance imaging. The depth where the fiber orientation became circumferential (0°) was 0.5 mm ~0.8 mm in ROI-A, ROI-B, and ROI-D; where it was ~0.3 mm in the posterior sector of the left ventricle (ROI-C). In all ROIs, the rate of fiber orientation changing with depth was faster at depths close to the epicardium, which was consistent with previous results obtained in a detailed histology study [1]. Quantitatively, the

#195629 - $15.00 USD Received 12 Aug 2013; revised 13 Oct 2013; accepted 15 Oct 2013; published 21 Oct 2013

fiber orientation increased with transmural depth at an average rate of 77°/mm, 73°/mm, and 86°/mm at the anterior (ROI-A), lateral (ROI-B), and posterior (ROI-C) part of the left ventricle, respectively. These values were similar to those reported in a DTI study of mouse heart [15].

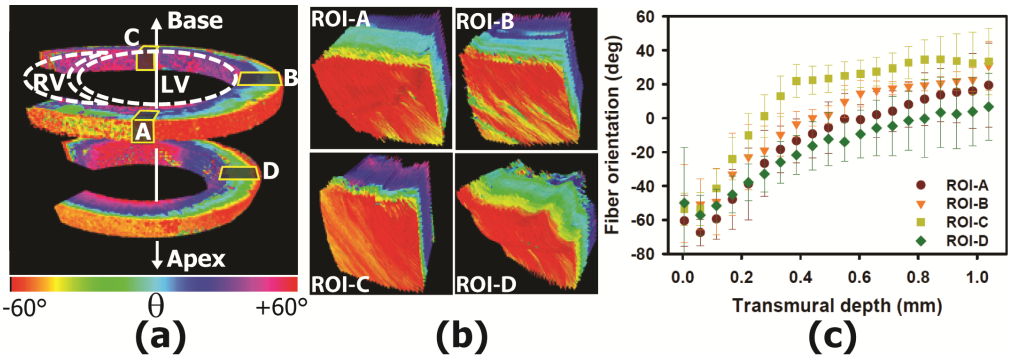

Fig. 4. (a) Four ROIs were extracted from different locations of the mouse heart. ROI-A, ROI-B, and ROI-C were located around the mid-heart of the left ventricle; while ROI-D was close to the apex of the heart. These ROIs had a size of 0.95 mm × 12° (B-scan by C-scan). (b) 3D color-coded tractography of the four ROIs. (c) The average fiber orientation as a function of transmural distance from the heart surface. Error bars shown represent standard deviations.

The standard deviation of fiber orientation within these ROIs ranged between 8° and 20°, which are similar to those previously reported in DTI and histological studies [18, 19]. In our results, fiber orientation usually had larger variation at depths greater than 0.9 mm from the epicardium due to degraded signal-to-noise ratio (SNR). Fiber orientation also showed larger variations at locations close to the heart surface. The fiber orientation actually showed a sudden trend change from decreasing to increasing with depth at ~50 μm from the outer surface (Fig. 4(c)). Similar abrupt changes in fiber orientation were reported previously at locations close to epicardium in large animals such as canines [18]. This phenomenon was related to the dense pericardium layer covering the outside wall of the heart. The pericardium layer was portrayed in the structural OCT image as a thin layer with very high reflectance. This phenomenon was not reported in existing DTI studies of mouse hearts most likely due to the insufficient spatial resolution in existing DTI systems.

4. Conclusion

In summary, we developed a new scanning and image reconstruction procedure for acquiring tractography in whole mouse hearts. The "cross-helical" laminar structure of myocardial fibers was clearly visualized using this technology. The obtained myocardial fiber organization was in accordance with existing knowledge acquired using diffusion tensor magnetic resonance imaging. Although the imaging depth of our current PSOCT system was not able to penetrate the entire heart wall (1.5 – 1.8 mm) [15] in mice, it was sufficient to cover the majority of the heart wall from the surface. The imaging depth may be improved by using an incident light at longer wavelengths such as 1060 nm or 1300 nm. Nevertheless, the micrometer scale resolution achieved by OCT is superior to that obtained in DTI and approaches the capability of histological imaging. Moreover, the fast imaging speed of current OCT technologies far exceeds the speed of DTI and histology analysis. Therefore PSOCT may become a valuable tool for studying myocardial microstructures in small animals.

Acknowledgments

We thank Dr. Shinghua Ding for providing mouse heart samples.

#195629 - $15.00 USD Received 12 Aug 2013; revised 13 Oct 2013; accepted 15 Oct 2013; published 21 Oct 2013